1 **Semiconductor/boron nitride composites: synthesis, properties, and**

2 **photocatalysis applications**

3 Chengyun Zhou[1], Cui Lai[1], Chen Zhang[1], Guangming Zeng[*], Danlian Huang[*], Min

4 Cheng, Liang Hu, Weiping Xiong, Ming Chen, Jiajia Wang, Yang Yang, Longbo

5 Jiang

6 *College of Environmental Science and Engineering, Hunan University and Key*

7 *Laboratory of Environmental Biology and Pollution Control (Hunan University),*

8 *Ministry of Education, Changsha 410082, P.R. China*

9

[*] Corresponding author at: College of Environmental Science and Engineering, Hunan University, Changsha, Hunan 410082, China.

Tel.: +86–731– 88822754; fax: +86–731–88823701.

E-mail address: zgming@hnu.edu.cn (G.M. Zeng), huangdanlian@hnu.edu.cn (D.L. Huang).

[1] These authors contribute equally to this article.

Contents

31 **Abstract**

32 Semiconductor photocatalysis has been regarded as one of promising approach to

33 solve the environmental pollution and energy crisis. Boron nitride (BN), as a new

34 nanomaterial, has distinct structures and properties that can add attractive properties

35 to photocatalysts. In the past few years, many encouraging achievements have been

36 made in the research field of BN-based semiconductor photocatalysts.

37 Semiconductor/BN composites have attracted extensive attention due to its well

38 photocatalytic activity. This work summarized recent progress on the synthesis of BN

39 and semiconductor/BN composites. These semiconductor/BN composites have

40 various applications in photocatalytic fields, such as pollutant degradation and

41 photocatalytic hydrogen evolution. The role of BN in semiconductor/BN composites

42 is discussed in depth. Coupling BN with semiconductors can improve the

43 photocatalytic activity of semiconductors due to their surface charge transfer

44 properties. The photocatalytic mechanism and different types of photocatalysts are

45 studied. Furthermore, perspectives on semiconductor/BN composites are discussed,

46 including the challenges for large scale preparations and theoretical calculation of

47 composites. It is expected that this review would be helpful for designing of highly

48 efficient semiconductor/BN composites.

49 Key words: Boron nitride; Semiconductor photocatalysis; immigration of electrons

50 and holes; Pollutant degradation

51

1. Introduction

Sustainable supply of green energy and environmental pollution are two of the main global challenges of the current era. Clean and safe water is an essential resource for the life and health for human [1-6]. However, around 1.2 billion people still have insufficient amounts of this resource around the world [7, 8]. With the fast industrialization development, more and more wastewaters containing organic pollutants and heavy metals was produced, which caused serious threats to the environment and drinking water [9-14]. These contaminants are resistant to conventional water and wastewater treatment, which may pose risks to human and ecological systems even at trace level [15-20]. Advanced Oxidation Processes (AOPs) was regarded as an effective technique for the degradation of organic contaminants, owing to the creation of highly reactive radicals (e.g. •OH, •O_2^-, and •SO_4^{2-}) [21-24]. Lately, visible light response photocatalysts arouse enormous attention for applications in environmental and energy areas.

Semiconductor based photocatalysis is one of the most promising technologies to solve the energy and environmental crisis [25-27]. A number of photocatalysts were synthesized and used for light induced chemical transformations, such as ZnO [28], TiO_2 [29, 30], CdS [31], and g-C_3N_4 [32-36]. When the photon energy of light is higher than the band gap of photocatalyst, electrons can be excited and transferred from the valence band (VB) to the conduction band (CB), leading to electron-hole separation. These charge carriers will migrate to the surface to initiate the chemical reaction [37, 38]. Photogenerated holes and electrons could be utilized for contaminants degradation, water splitting, and disinfection. However, the charge carriers can easily recombine. The emerging nanomaterials as the new building blocks

4

76   to construct light energy harvesting assemblies has opened up new ways to utilize

77   renewable energy resources due to their large surface areas, abundant surface states,

78   and diverse morphologies.

79   Among them, hexagonal boron nitride (h-BN), a two-dimensional (2D) network of

80   hexagonal structured material, has attracted a lot of research interest [39, 40]. The

81   h-BN is composed of equal numbers of boron (B) and nitrogen (N) atom, and it was

82   thought to be a type of synthetic material [41, 42]. The h-BN is called "white

83   graphene" or "non-carbon graphene" due to the analog 2D atomic crystal structure

84   and van der Waals heterojunction [43, 44]. The h-BN possesses a high thermal

85   conductivity (600 W m^{-1} K^{-1}), a wide band gap (5.2-5.5 eV) and a high surface area

86   (3300 m^2 g^{-1}) [45]. These unique properties indicate that h-BN has great potential to

87   be applied in adsorption [46-48], energy storage [49-51], and catalysis [52-54]. With

88   the rapid development of h-BN preparation technology, the h-BN based nanomaterials

89   for applications in photocatalytic field are also under fast development. Many

90   important findings have been reported on the h-BN based nanomaterials during the

91   past few years, such as TiO_2/h-BN [55, 56], g-C_3N_4/h-BN [57]. BN-based

92   photocatalysts present higher photocatalytic activity than its single photocatalyst due

93   to their surface properties. The photocatalytic enhancement is generally ascribed to

94   the suppressed recombination of photogenerated electron–hole pairs, extended

95   excitation wavelength and increased surface-adsorbed reactant. As the field of

96   semiconductors/h-BN composite advancing, a comprehensive review regarding on the

97   latest developments is necessary and urgent at this stage.

98   In this review, we briefly introduce the fabrication of the BN and BN-based

99   materials, followed by placing emphases on recent development about the

5

100   applications of BN-based materials as catalysts in the environmental remediation and

101   energy conversion. Finally, the challenge and perspectives for future development are

102   discussed. We hope that this paper would be helpful for designing and fabricating

103   novel semiconductor/BN photocatalysts with greater performances in the near future.

104   **2. Syntheses of BN and semiconductor/BN composites**

105   2.1 Syntheses of BN

106   Boron is a lightweight and metalloid element that is generally capable of forming

107   stable covalent bonds in crystalline structures with boron in the oxidation state III. BN

108   is the most promising and popular inorganic nonmaterial [58,59]. Recently, BNs have

109   been discovered in natural mineral and in several different forms, including

110   graphite-like hexagonal boron nitride (g-BN or h-BN), cubic boron nitride (c-BN),

111   wurtzite boron nitride (w-BN), and amorphous boron nitride (a-BN). Among these

112   forms, the h-BN is the representative crystal structures of BNs [60]. To date, many

113   methods have been applied in the preparation of BN, which have similarities to the

114   methods used to fabricate graphene, including ball milling, template approach, and

115   template-free approach. Different synthetic methods for BN materials have been

116   summarized in Table 1. To achieve better dispersion and enlarge the application of

117   BN, methods like chemical modification have been employed.

118   2.1.1 Mechanical exfoliation technique

119   Mechanical exfoliation technique was often used to separate the multilayer

120   grapheme [61]. Layered h-BN nanosheet can also be prepared by this technique. Urea

121   was employed to assist exfoliation of the h-BN by ball milling method. This ambient

122   temperature method has several advantages, including scalability for mass production,

123 low cost, high yield without organic solvents. Similarly, Lee et al. prepared

124 hydroxyl-functionalized BN nanoplates (OH-BNNPs) by a simple ball milling of BN

125 powders in the presence of sodium hydroxide (Fig. 1a) [62]. Fig. 1b shows

126 low-magnification TEM images indicating that there are thin 2D nanoplates in

127 solution. The inset figure shows selected area electron diffraction (SAED) pattern

128 measured along the (0001) zone axis, which exhibits typical 6-fold symmetry of h-BN,

129 suggesting that the hexagonal lattices of the OH-BNNPs were not damaged during the

130 exfoliation processes.
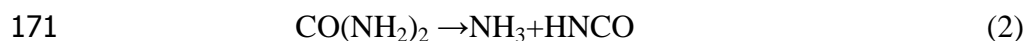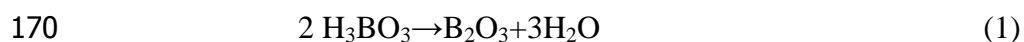
131 2.1.2 Template approach

132 The template approach is the most widely reported and successfully used method

133 for the introduction of mesoporous in solid materials such as carbon, polymers and

134 ceramics [63, 64]. For example, Bios et al. primarily prepared a ordered mesoporous

135 boron nitride (MBN) by using CMK-3 mesoporous carbon as a template and

136 tri(methyl-amino)borazine as a boron nitride source [65]. The specific surface area

137 (540 m^2 g^{-1}), and the mesoporous volume (0.27 cm^3 g^{-1}) of BN are higher than that of

138 the non-porous BN. Vinu et al reported the preparation of mesoporous boron nitride

139 (MBN) with a very high surface area and pore volume [66]. The materials were

140 fabricated via substitution reactions at high temperatures (1500 to 1750 ℃), using a

141 well-ordered hexagonal mesoporous carbon as a template and boron trioxide as a

142 boron source. The specific surface area and the specific pore volume of MBN are 565

143 m^2 g^{-1}, and 0.53 cm^3 g^{-1}, respectively. Schlienger et al. prepared MBN-based materials

144 template of zeolites [67]. The overall synthetic path of zeolite-derived BN-based

145 materials was presented in Fig. 2. Maleki et al. developed a facile procedure for the

146 synthesis of BN with hierarchical porous structure using CTAB and PS as dual

147 inorganic templates [68].

148   Soft template approach is also an interesting strategy, which has been applied for

149 the synthesis of various porous BN materials. Block polymers such as P123 and P127

150 have been used in the preparation of BN materials. Li et al. demonstrated that the

151 mixture of P123 and BN precursors (Boric acid and melamine) could obtain the

152 porous ribbon-like microstructure BN [69]. The BET surface area of BN was found to

153 be 2700 m^2 g^{-1}, and the pore volume was up to 1.66 cm^3 g^{-1}. The addition of P123 in

154 this work not only increases the surface area and pore volume but also enhances the

155 adsorption ability of the pristine BN. The porous BN can be as a promising material

156 applied for environmental remediation.

157 2.1.3 Template-free approach

158   Hard or soft templates have many disadvantages, such as tedious synthesis

159 procedures, difficult in removing the template completely, long preparation time and

160 high cost, which limit their extensive applications in a large-scale. Recently, a variety

161 of porous BN with different structure and morphology have been synthesized by the

162 self-assembly and template-free methods [70, 71]. Nag and co-workers demonstrated

163 that the thin graphene analogue BN layers could be obtained via the polymerization of

164 boric acid and urea at 900 ℃ in N_2 atmosphere [72]. The surface area of the BN can

165 be controlled by the layer thickness. When the ratio of boric acid to urea is 1 to 48, the

166 sample could achieve the thinnest BN layer with a surface area of 927 m^2 g^{-1} and a

167 high CO_2 uptake. This simple method has enabled us to prepare graphene analogue

168 BN with varying thicknesses. The details of the reaction are explained by the

169 following equations (Eq. (1)-(3)).

8

$$170 \qquad 2 H_3BO_3 \rightarrow B_2O_3 + 3H_2O \qquad\qquad (1)$$

$$171 \qquad CO(NH_2)_2 \rightarrow NH_3 + HNCO \qquad\qquad (2)$$

$$172 \qquad B_2O_3 + 2NH_3 \rightarrow 2BN + 3H_2O \qquad\qquad (3)$$

173   Interestingly, Wu et al. recently synthesized h-BNs with varying surface areas

174 relying on the solvents used during the preparation steps of the precursors [70].

175 Solvents and drying time had an effect on the crystalline structure of the intermediates

176 [73]. For example, Marchesini and co-workers have developed a template-free

177 method to produce BN with tunable surface area and micro/mesoporosity by using

178 multiple N-containing precursors in Fig. 3 [74]. The optimized sample exhibit a

179 surface area of 1400 m^2 g^{-1} and enhanced CO_2 capture capacity compared to

180 commercial zeolites. In addition, the BN can be shaped as pellets with little or no

181 reduction in porosity and gas uptake.

182   In addition, Lei et al. synthesized highly porous BN nanosheets by the simple

183 thermal condensation of boron trioxide and guanidine hydrochloride [60]. The

184 mixture was heated in a flowing nitrogen-15% hydrogen atmosphere at 1100 ℃ for

185 2h. The resulting product could exhibit a high surface area of 1427 m^2 g^{-1} and a pore

186 size distribution ranging from 20 to 100 nm. The material shows excellent sorption

187 performances for a wide range of oils, solvents and dyes, with mass uptakes reaching

188 3,300%, which was due to a combination of super hydrophobicity, porosity and

189 swelling ability.

190 2.2 Syntheses of semiconductor/BN composites

191   A variety of semiconductors have been employed to the synthesis of

192 semiconductor/BN composites, such as metal oxides and metal sulfides (e.g. TiO_2,

193   ZnO, WO$_3$ and CdS), bismuth based semiconductor (e.g. BiOBr, BiOCl, Bi$_4$O$_5$Br$_2$,

194   and BiOI), and silver based semiconductor (e.g. AgI, AgBr, Ag$_3$PO$_4$, AgVO$_4$, and

195   AgCrO$_4$) and metal-free semiconductor (e.g. graphitic carbon nitride). The widely

196   preparation methods are including *in-situ* growth, precipitation, ball milling,

197   hydrothermal and/or solvothermal method, which are summarized in Table 1. Here,

198   the following passages will give a more detailed description of the available synthesis

199   routes.

200   2.2.1 *In-situ* growth method

201   The *in-situ* growth method is widely used to prepare the BN based composites.

202   The precursor of metal salt could be transformed into metal oxides and then deposited

203   on the surface of BN, and then forming the BN based composite. Tang et al.

204   constructed BN/TiO$_2$ composite through the hydrolysis of TiCl$_3$ in the ethanol-water

205   aqueous solution with BNNTs [75]. This method involves the reaction of Ti^{3+} with the

206   oxidized radicals BN-H$^+$ to form BN/Ti^{4+} bonds firstly, and *in-situ* hydrolytic

207   conversion of the attached Ti^{4+} into TiO$_2$. Ide et al. also used TiCl$_3$ as precursor and

208   *in-situ* growth TiO$_2$ with BN [76]. Then, the Au/TiO$_2$/BN could be obtained through

209   the HAuCl$_4$ 3H$_2$O and the as-prepared TiO$_2$/BN. Tetrabutyl titanate (Ti(OC$_4$H$_9$)$_4$) is

210   another precursor of TiO$_2$. For example, BN/TiO$_2$ composites were fabricated via

211   water-phase synthesis by Liu et al., who used porous BNNSs and Ti(OC$_4$H$_9$)$_4$ as the

212   starting materials [77]. After stirring and heating, the TiO$_2$ nanoparticles were

213   deposited on the surface of the BN as it is hydrolyzed. As shown in Fig. 4, The TEM

214   image of porous BNNSs/TiO$_2$ (38 wt%) hybrid nanosheets shows that the TiO$_2$

215   nanoparticles were loaded homogenously on porous BNNSs. The HRTEM image of

216   TiO$_2$ nanoparticles indicated a well-defined crystallinity of TiO$_2$ with lattice spacing

217 of 0.355 nm, which corresponded to the (101) planes of anatase phase. In addition,

218 Wang and co-workers developed a facile *in-situ* growth method with the hydrolysis of

219 $SnCl_2$ in the presence of BN acid aqueous solution to obtain the BN/SnO_2 composite

220 [78]. The *in situ* growth strategy can avoid the agglomeration of the semiconductor

221 nanoparticles on the BN.

222 A variety of silver-based semiconductor photocatalysts can also be immobilized

223 on to BN materials by *in-situ* growth strategy. For example, Choi et al. prepared a

224 two-component composite of AgI/BN by an *in-situ* ultrasound assisted method. They

225 added an aqueous solution of BN and $AgNO_3$ dropwise into a BN solution [79]. AgI

226 was formed at the surface of BN sheets at room temperature. In order to get enhanced

227 photocatalytic activity of AgI/BN photocatalyst, Wu and co-workers synthesized a

228 navy bean shaped AgI/AgBr biphasic heterostructures loaded on few-layered h-BN

229 nanosheets [80]. The BN and AgBr were first dispersed in deionized water and

230 sonicated. Then KI aqueous solution was added into the mixture solution and stirred

231 for anion exchange. Polyvinyl pyrrolidone (PVP), as an excellent dispersant, was to

232 protect the silver nanoparticles from growing and agglomerating [81]. Zhu et al.

233 deposited Ag_3PO_4 nanoparticles on the h-BN nanosheets via the simple precipitation

234 method [82]. Amount of h-BN and PVP were suspended in aqueous solution, and then

235 the $AgNO_3$ aqueous solution and Na_2HPO_4 aqueous solution were added into the

236 above h-BN solution under dark condition. Apart from this material, other silver

237 based BN composites have been prepared via this method, such as BN/AgBr [83],

238 $BN/AgCrO_4$ [84], BN/Ag_2CO_3 [85], and BN/Ag_3VO_4 [86].

239 Graphene carbon nitride (g-C_3N_4), a non-metal material, is regarded as a

240 promising visible light driven photocatalyst. The catalytic performance of g-C_3N_4 can

be improved by the hybridization with other 2D materials, such as graphene and its derivatives. Recently, our group prepared the g-C_3N_4/BN composites by a facile in-situ growth strategy [87]. We used h-BN and dicyandiamide as precursor, calcined at 550 °C, and then g-C_3N_4/BN was obtained. g-C_3N_4 was deposited on the surface of BN sheets due to the π-π interaction of structure between g-C_3N_4 and BN. Very recently, He and co-worker reported the direct growth of g-C_3N_4 on the h-BN porous nanosheets [88]. The g-C_3N_4/ h-BN composite was obtained by using the boric acid and urea as the source of h-BN, and using urea as precursors of g-C_3N_4.

2.2.2 Ball milling method

Ball-milling is a very effective method to prepare the solid–solid composites, which can enhance the reactivity of the reagents due to mechanical breaking of molecular bonds. Ball-milling has been used to prepared photocatalyst composites. Since the BN is formed by the rolling up of sheet, more accessible layer structure may achieve better electrostatic distribution. Chen et al. used water as solvent and different contents of BN to prepared h-BN/TiO_2 via ball milling [89]. Through milling process, the h-BN and TiO_2 can be connected closely, and then the charged h-BN could promote the immigration of holes from the bulk of TiO_2 to its surface. Similarly, Fu et al. also fabricated the h-BN/ZnO by these above methods [90]. For further restrain the recombination of photogenerated electron–hole pairs of CdS, it is also possible to use the exfoliated h-BN as the holes capturer. Zhang et al. synthesized the BN/CdS composite samples by ball milling method [91]. The bulk h-BN was milled into some flake and was combined with CdS in the ball-milling process.

2.2.3 Solvothermal/hydrothermal method

The solvothermal method is an effective approach to the preparation of semiconductors/BN composites. Recently, Xie et al. found a route for the preparation of TiO_2/BN with the hydrothermal method using the ethanol as solvent [92]. Considering the poor dispersion of h-BN in water, ionic liquid was added to improve the dispersion. The BN/$BiPO_4$ composite was obtained when $Bi(NO_3)_3 \cdot 5H_2O$ and ionic liquid (Omim H_2PO_4) was mixed with BN nanosheet in ethanol and heated at 160℃ for 24 h in oven [93]. Similarity, A graphene-like BN modified BiOBr materials were also fabricated by 1-hexadecyl-3-methylimidazolium bromide (C_{16}mim Br) ionic liquid assisted solvothermal method [94]. In addition, the BN based composites with distinct morphology has also been prepared by this method [95]. For example, Liu et al. fabricated 3D hierarchical microsphere BN/BiOI composite by a solvothermal method [96]. Other Bi-based semiconductors have also been integrated with BN by this method, such as Bi_2WO_6, and $Bi_4O_5Br_2$. For example, Ding et al. synthesized the h-BN/$Bi_4O_5Br_2$ via a facile micro emulsion/hydrothermal method with TX-100 as surfactant emulsion in Fig. 5 [97].

Hydrothermal method is also versatile for the application of 2D BN nanosheets coupled metal sulfides, such as BN/In_2S_3 [98], BN/CdS, BN/$Cd_xZn_{1-x}S$ and BN/$ZnIn_2S_4$ [99]. For example, the BN/In_2S_3 composite was fabricated through one-pot hydrothermal method by heating a mixture of $InCl_3.4H_2O$ and thiacetamide on the surface of BN nanosheet [98]. Similarly, a simple hydrothermal method was also employed to obtain the a-BN/CdS [99]. Very recently, Gu et al. prepared 2D BN/g-C_3N_4 composite through a hydrothermal method, wherein a mixture of BN, NH_4Cl and g-C_3N_4 in water was heated for 12 h at 180 ^{o}C in an autoclave [100]. Solvothermal/hydrothermal methods were attractive to researchers owning to some advantages, such as mild reaction condition and simple control of reaction.

289 2.2.4 Thermal condensation process

290   Thermal condensation process is another method for preparation of

291 semiconductor/BN composites. Sun et al. employed a thermal treatment to embed Pt

292 NPs into hexagonal boron nitride (h-BN) layers [101]. The Pt@h-BN was synthesized

293 by hydrogenation of NH_3BH_3 on the surface of Pt and then heated at 500 or 700 ^{o}C

294 for 2h in flowing NH_3. Similarly, this method can also be developed to encapsulate Ni

295 NPs with few-layer h-BN shells. Gao et al. prepared the Ni@h-BN via the above

296 method [102]. Firstly, a carbon support mixed with nickel nitrate ($Ni(NO_3)_2$) and

297 boric acid (H_3BO_3) solutions was synthesized. Then, the mixture was heated in an

298 autoclave at 120 ^{o}C. The obtained product was then annealed in NH_3 at different

299 calcination time. From the XPS results, the graphitic h-BN shells can be synthesized

300 through the reaction between H_3BO_3 and NH_3 at 700 ^{o}C.

301   Thermal condensation process was also employed to prepare the BCN

302 composite. Qiu et al. fabricated the BCN via condensation [103]. Different amounts

303 of BH_3NH_3 were doped into the classical carbon nitride condensation. Huang et al.

304 introduced a novel and simple way of carbon doping of h-BN nanosheets to generate

305 ternary BCN as sustainable and stable visible light photocatalysts [104]. They placed

306 boron oxide, urea and a certain amount of glucose into the horizontal tube furnace.

307 Thaweesak et al. prepared BCN via a one-step thermal condensation process [105].

308 BNH_6 was first mixed with dicyandiamide and NH_4Cl, and then transferred into

309 alumina crucible at 600 ^{o}C for 4h under N_2 flow.

310 2.2.5 Other techniques

311   Electrospinning approach has been used to fabricate BN based nanocomposites.

312 Nasr et al. prepared the BN nanosheets/TiO_2 nanofibers via electrospinning technique

14

313   [106]. They used different amounts of boron nitride and absolute ethanol as spun

314   solution, and titanium tetraisopropoxid ethanol mixed with polyvinylpyrrolidon as the

315   precursor solution.

316   Microwave irradiation is a rapid and simple method to provide homogeneous

317   heating process for synthesis of nanocrystals with controllable size and shape on the

318   surface. It can be used for simultaneous formation of metal compounds and BN to

319   prepare BN based hybrids. Boron nitride (BN)-modified bismuth oxychloride (BiOCl)

320   materials have been synthesized via a facile microwave-assisted method [107].

321   $Bi(NO_3)_3 \cdot 5H_2O$ was first dispersed in glycerol solution, and a solution of NaCl was

322   added dropwise. Then the mixture was transferred into a three-necked flask, and the

323   reaction was carried out in microwave reactor at 1000 W and 140 °C for 1 h. This

324   method could reduce the reaction time and greatly improve the efficiency of
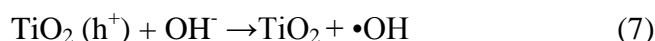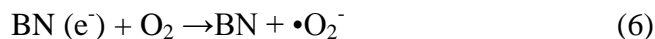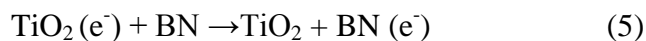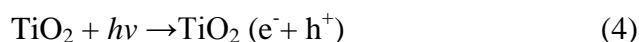
325   large-scale production.

326   **3. Semiconductor/BN composites in photocatalysis applications**

327   In recent years, semiconductor photocatalysts have been expected to play an

328   important role in solving many environmental and energy challenges. However, the

329   fast recombination rates of photogenerated charge carriers caused the low efficiency,

330   thus limiting its applications. Recently, semiconductor/BN composites have attracted

331   extensive attention due to its well photocatalytic activity. The composites could

332   potentially enhance the separating of electron-hole. Table 2 shows the applications of

333   semiconductor/BN composites, which exhibit enhanced photocatalytic degradation of

334   different target organic substrates. In addition, semiconductor/BN composites were

335   also employed for H_2 evolution under light illumination.

336   3.1 Metal oxide/BN and metal sulfide/BN composites

337   Among metal oxide/BN semiconductor systems, TiO_2/BN composites were very

338   attractive. TiO_2/BN composite was reported to have a high photocatalytic

339   performance for the degradation of methylene blue (MB), methyl orange (MO) or

340   rhodamine B (RhB). Mechanism revealed that the BN in the composites can promote

341   charge separation and increase the adsorption of pollutants. Singh et al. revealed that

342   the BN–TiO_2 showed an enhanced visible light photocatalytic activity for degradation

343   of MB in water [108]. The photodegradation rate of BN–TiO_2 is 79% in 200 min,

344   which is higher than that of TiO_2 (32%) in the visible region. MB molecules can be

345   transferred from the solution to the surface of TiO_2 and adsorb with offset face-to-face

346   orientation via π-π conjugation between MB and BN, and therefore, its adsorption

347   ability of dyes increases compared to that of the pristine TiO_2. Fu et al studied the

348   performances of h-BN/TiO_2 for the degradation of RhB and MB under UV light

349   irradiation [89]. The photocatalytic degradation rate of optimized h-BN/TiO_2

350   composite for RhB and MB was 15 and 8 times higher than the pristine TiO_2,

351   respectively. Also, BN nanofiber was also combined with TiO_2 due to electrostatic

352   attraction. The composite showed efficient photocatalytic decomposition of MO under

353   UV light [106]. The removal rate constant for the optimized composite was reached

354   0.0586 min^{-1}, which showed 5 and 3.8 times higher than that of P25 and TiO_2

355   nanofiber alone. Si and co-workers prepared the few-atomic-layer BN hollow

356   nanospheres for degradation of MO [109]. The shells of BN nanospheres only consist

357   of 2-6 layers. In Fig. 6, the TEM and HRTEM image showed that the TiO_2 was

358   dispersed on the surface of BN. The MO was completely degraded by the optimized

composite in 12 min. The reaction mechanism (Eq. (4)-(8)) involved in h-BN/TiO_2 is given below:

$$TiO_2 + h\nu \rightarrow TiO_2 \; (e^- + h^+) \qquad (4)$$

$$TiO_2 \; (e^-) + BN \rightarrow TiO_2 + BN \; (e^-) \qquad (5)$$

$$BN \; (e^-) + O_2 \rightarrow BN + \bullet O_2^- \qquad (6)$$

$$TiO_2 \; (h^+) + OH^- \rightarrow TiO_2 + \bullet OH \qquad (7)$$

$$\bullet OH + Pollutants \rightarrow Degradation \; products \qquad (8)$$

BN/TiO_2 not only has a good photocatalytic activity under UV light but also has good photocatalytic property under visible light. Nitrogen-doped TiO_2 ($TiO_{2-x}N_x$)/BN was explored for visible light driven degradation of RhB [110]. Compared with pure TiO_2 and $TiO_{2-x}N_x$ composite, the $TiO_{2-x}N_x$/BN composite exhibits much higher photocatalytic degradation activity. The degradation efficiency of RhB reaches 97.8% in 40 min. Gold nanoparticle-loaded TiO_2 (Au/TiO_2) as a visible light photocatalyst has attracted much attention. For example, Au/TiO_2/BN showed high photocatalytic activity towards the decomposition of crystal violet (CV) aqueous under solar light irradiation [76]. The apparent reaction rate constant for the optimized composite was estimated to be 10.3 μmol h^{-1}, which was higher than the pristine Au/TiO_2 (2.8 μmol h^{-1}). The role of BN in the Au/TiO_2/BN composite is to promote charge separation in TiO_2 and improve the adsorption ability of CV. Recently, Liu et al. demonstrated that the porous BN/TiO_2 hybrid was highly active for the degradation of RhB under visible light [77]. The porous BN/TiO_2 hybrid nanosheets (38 wt%) achieve a degradation percentage up to 99% within 6 h, which is much higher than that of P25 (60%).

382   Except TiO_2, other metal oxide (SnO_2, WO_3, ZnO, etc) photocatalyst and its

383   modified materials also have many potential applications in photocatalysis. BN with

384   its large surface area can serve as a good adsorbent to gather pollutants around the

385   semiconductor particles [111]. Moreover, fabrication of heterojunction with BN is

386   beneficial for enhancing them separation of electron-hole pairs. Wang et al. evaluated

387   the visible light photocatalytic activity of SnO_2/BN for degradation of methyl orange

388   (MO) in water [78]. The degradation efficiency of MO by SnO_2/BNMB reached 92%

389   after 30 min under visible light irradiation, whereas the pure SnO_2 was inactive for the

390   degradation of MO. The improved photocatalytic activity of SnO_2/BNMB was

391   because the optical absorption of SnO_2 and the strong adsorption activity of the support

392   h-BN. A similar mechanism has also been put forward for RhB degradation over

393   BN/WO_3 under visible light irradiation [112]. Xu et al. reported the BN/WO_3

394   composite as a visible light photocatalyst. The hybrid composite exhibited enhanced

395   photodegradation efficiency for RhB. The apparent reaction of the composite was

396   estimated to be 0.6327 h^{-1}, which was 2.8 times higher than the pure WO_3. Fu et al.

397   found that the photocatalytic activity of ZnO can be also improved by coupling with

398   h-BN [90]. For h-BN (1.0 wt%)/ZnO, the degradation efficiencies of RhB and MB

399   reach to 82% and 60% under 20 min irradiation, respectively. While the

400   corresponding degradation efficiencies are 33% and 30% for pure ZnO, respectively.

401   The enhancement activity of h-BN/ZnO is attributed to the negatively charged h-BN

402   surface, which can promote the transfer of the photoinduced holes to ZnO surface and

403   facilitate the adsorption of cationic dyes around ZnO.

404   Metal sulfide semiconductors have attracted tremendous attention owing to their

405   superior electrical and optical properties. CdS, as one of the narrow bandgap

406   semiconductors (2.2–2.4 eV), exhibits high optical response and has been widely

18

407 applied as a photoharvester for photocatalysis. However, the photocorrosion effect

408 makes CdS unstable as a photocatalyst thereby greatly limited its practical application.

409 CdS can be combined with BN to assemble CdS/BN composite for H_2 evolution. For

410 example, Zhang and co-workers fabricated the ternary Pt/BN/CdS composites for

411 visible light driven H_2 production from water [91]. For the composite with 5.0 wt%

412 BN, the evolution rate of H_2 can be reached as high as 17.56 mmol g^{-1} h^{-1} which was

413 about 3 times higher compared with the Pt/CdS. The heterojunction between BN and

414 CdS was important for the separation of photogenerated charge carriers, this effect

415 can be enhanced the photocatalytic activity of BN/CdS. Lately, Ma et al. fabricated

416 CdS/hexagonal boron nitride nanosheets (BNNSs) and applied it to hydrogen

417 evolution [113]. The rate of H_2 evolution on 0.5 wt% CdS/BNNSs was 439.4 μmol

418 g^{-1} h^{-1}, which was 2.3 times higher than that of the pure CdS. It can be found that the

419 rate of H_2 evolution on Pt/CdS/BNNSs was 5.961 mmol g^{-1} h^{-1} when Pt was loaded.

420 BNNSs were inactive for H_2 evolution but it can offer a large surface for catalytic

421 reaction. In addition, the well connection of BN and CdS broaden the

422 photo-absorption region and enhance electronic communication of CdS, which make

423 the enhancement of photocatalytic H_2 evolution.

424 3.2 Silver based semiconductor/BN composites

425 Recently, silver based semiconductors exhibit promising photocatalytic activity

426 for the water splitting and removal of organic pollutants. BN can be coupled with the

427 silver based semiconductor for the enhancement of photocatalytic activity. Ag_3PO_4

428 has high photo-oxidative activity under visible light irradiation but it is susceptible to

429 corrosion. Zhu et al. constructed the BN/Ag_3PO_4 for MB degradation under visible

430 light irradiation [114]. The degradation rate constant of MB by 1% BN/Ag_3PO_4 was

about 2.79 times higher than that of pure Ag_3PO_4. The excellent photocatalytic activity of BN/Ag_3PO_4 was ascribed to the high separation efficiency of photogenerated electrons between the BN and Ag_3PO_4. The superior electron-hole separation efficiency of BN/Ag_3PO_4 was examined by photoluminescence spectra, electrochemical impedance spectroscopy and transient photocurrent responses experiments. A similar mechanism was also obtained by $h-BN/Ag_3VO_4$, BN/Ag_2CO_3 and $Ag_2CrO_4/FBNNS$ [84]. Lv et al. reported the RhB photocatalytic degradation rate constant of $h-BN/Ag_3VO_4$ was 0.0384 min^{-1}, which was about 6 folds that of pure Ag_3VO_4 (0.0062 min^{-1}) [86]. Also, the results of RhB degradation showed that the removal rate of 3 wt% BN/Ag_2CO_3 was almost 1.24 times higher than pure Ag_2CO_3 under visible light irradiation [85].

Silver halides (e.g., AgBr and AgI) are well known as photosensitive materials in photography and display high photocatalytic activity. Coupling BN with silver halides to form composites, such as BN/AgBr, AgI/BN and AgI/AgBr/h-BN have been found to be enhanced the photocatalytic activity of bulk material [83]. Choi et al. studied the effectiveness of BN/AgI composite for the decomposition of RhB under visible light irradiation [79]. The 2 wt% BN/AgI composite exhibited a significantly higher activity than that of the bare AgI. Moreover, the composite exhibited good photostablity, which showed a degradation efficiency of 87.8% after 5 successive experimental runs. This enhanced photoactivity and stability of AgI/BN may be attributed to the effect of heterojunction between AgI and BN. On the basis of BN/AgI, Wu et al. constructed the heterostructured AgI/AgBr/h-BN composite for degradation RhB and MO [80]. The formation of AgI/AgBr navy beans could promote the separation of photogenerated electron-hole pairs. Under visible light irradiation, the photocatalytic activity was in the order AgI/AgBr/h-BN > AgI/AgBr >
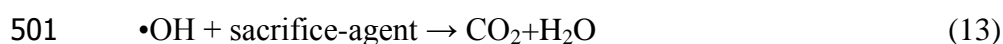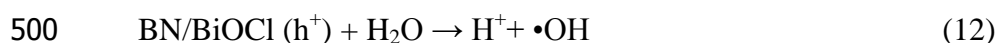
20

456 AgBr. The photogenerated electron of AgI could be injected into the CB edge of

457 AgBr, and then the electrons could be effectively transferred to the surface of h-BN

458 and further could be turned into superoxide radical on the surface of the catalyst.

459 3.3 Bismuth-based semiconductor/BN composites

460 Bismuth based semiconductors such as BiOX (X=Br, Cl and I) [94, 96], $Bi_4O_5I_2$

461 [115], $Bi_4O_5Br_2$ [97], Bi_2WO_6 [116] and $BiPO_4$ [93] have emerged as attractive

462 materials in various photocatalytic applications. Bismuth based semiconductors were

463 also demonstrated for integration with BN for photocatalytic degradation of organic

464 pollutants. When 0.5 wt% BN was loaded in BiOI, a significant improvement of the

465 photodegradation activity of RhB could be observed to contribute to the performance

466 by a factor of 2. The results were presented in Fig. 7a and 7b [96]. The heterojunction

467 mechanism between the BN and BiOI was proposed for the improved activity. Similar

468 to BiOI, BiOBr was also proven to conjugate with BN for photocatalytic degradation.

469 Di and co-worker demonstrated that the 1 wt% BN/BiOBr composite presented

470 enhancement for the photodegradation of RhB, ciprofloxacin (CIP), and tetracycline

471 hydrochloride (TC) under visible light driven [94]. As shown in Fig. 7c and 7d, nearly

472 81.5% of CIP was degraded after 90 min by 1 wt% BN/BiOBr, while only 57.3%

473 degradation was achieved by pure BiOBr. The variation in photocatalytic efficiency

474 was attributed to the improved visible light harvesting ability and high separation

475 efficiency of photogenerated electron–hole pairs. In addition, Ding et al. construct the

476 heterojunction photocatalyst h-BN/$Bi_4O_5Br_2$ for degradation 4-tert-Butylphenol

477 (PTBP) [117]. The optimum amount of loaded h-BN is 1 wt%, and the

478 photodegradation followed first-order kinetics with a reaction rate constant of 0.02

479 min^{-1}, which was 4 times larger than that of the pure $Bi_4O_5Br_2$. As shown in Fig. 8a-e,

density functional theory (DFT) calculations revealed that h-BN/$Bi_4O_5Br_2$ would reduce the hybrid electron density of h-BN in the CB, and thus the CB electrons of h-BN migrate to the surface of $Bi_4O_5Br_2$, preventing recombine of electron-hole pairs.

In contrast to organic pollutants, inorganic metal ions are problematic since they are not biodegradable and endanger the living organisms. Hexavalent chromium (Cr^{6+}) is a common pollutant from mining industry and electroplating industry, which is a significant threat to human health. In contrast, Cr^{3+} is an essential trace element and required for human health. Hence, reduction of Cr^{6+} to Cr^{3+} is an effective method of controlling its pollution. Photocatalytic reduction is considered as a promising method owing to its low cost and environmental friendly [118]. Xu et al. studied the photoactivity of g-BN-decorated BiOCl microspheres for Cr^{6+} reduction upon visible-light irradiation [118]. The prepared 1% BN/BiOCl materials exhibited an up to 2.03-fold enhanced Cr^{6+} reduction rate constant compared with pure BiOCl microspheres due to the suppressed recombination of photogenerated electron–hole pairs. The mechanism was presented in the following equations (Eq. (9)-(13)). Also, Xie et al. reported TiO_2/h-BNNSs showed an enhanced photocatalytic activity for simultaneous removal of dyes (Lanaset Red50, LR2B) and Cr^{6+} [119].

$$BN/BiOCl + hv \rightarrow BN/BiOCl\ (e^- + h^+) \qquad (9)$$

$$BN/BiOCl\ (e^- + h^+) + g\text{-}BN \rightarrow g\text{-}BN\ (e^-) + BN/BiOCl\ (h^+) \qquad (10)$$

$$g\text{-}BN\ (e^-) + Cr_2O_7^{2-} + H^+ \rightarrow Cr^{3+} + H_2O \qquad (11)$$

$$BN/BiOCl\ (h^+) + H_2O \rightarrow H^+ + \bullet OH \qquad (12)$$

$$\bullet OH + sacrifice\text{-}agent \rightarrow CO_2 + H_2O \qquad (13)$$

3.4 g-C_3N_4/BN composites

503   Metal free photocatalyst graphene carbon nitride (g-C_3N_4) was proposed by Wang

504   et al. in 2009 [120]. The band gap of g-C_3N_4 was 2.5-2.7 eV [121, 122]. The few-layer

505   BN nanosheets were well-attached to the g-C_3N_4 to establish sufficient contact

506   interface in the 2D/2D construction between the two materials. Gu et al. introduced

507   the BN on the surface of g-C_3N_4 to form the nanocomposite in Fig. 9a [100]. The

508   optimized 0.5% BN/g-C_3N_4 sample presented the highest photocatalytic activity

509   towards RhB degradation, which can achieve the high efficiency of 98.2% within 120

510   min. Recently, our group also reported that the 0.48% h-BN/g-C_3N_4 (denoted as BC-3)

511   nanocomposites showed higher photocatalytic activity towards RhB and TC

512   degradation compared to g-C_3N_4 [123]. It was observed that 98.5% of RhB was

513   decomposed in 40 min, while 80.5% of TC was degraded after 1 h over BC-3. The

514   superior photocatalytic activity of h-BN/g-C_3N_4 composites could be caused by the

515   larger surface area and higher separation efficiency of electron–hole pairs. The

516   degradation mechanism was proposed in Fig. 9b.

517   Loading g-C_3N_4 on h-BN sheets can also improve the photocatalytic activity for

518   the H_2 evolution. For example, He et al. successfully demonstrated the enhanced

519   photocatalytic activity of CN/h-BN (CBN-x) for the H_2 production [57]. Fig. 10a

520   shows that the CBN-6 was composed of 4-6 layers and has a porous structure. The

521   HRTEM image revealed the layered CN was formed on h-BN surface (Fig. 10b). It

522   was found that CBN-6 is more effective than BN for the photocatalytic H_2 evolution

523   (Fig. 10c). The band gap of CBN is gradually reduced by loading of CN (Fig. 10d). In

524   such system, the photogenerated electrons of CN could transfer to the conduction

525   band of BN, while the holes of BN are transferred into the CN phase to achieve better

526   charge separation and prolong the lifetime of the electrons.

4. Role of BN in semiconductor/BN composites

BN can accept photogenerated electrons from the CB of most semiconductors, which will efficiently suppress the recombination of photogenerated charges and enhance their photocatalytic degradation activity. The role of BN as an electron acceptor and transporter has been extensively discussed. For example, when the h-BN was coupled with Ag_3VO_4, the electrons in Ag_3VO_4 could transfer to the h-BN for the interfacial interaction between BN and Ag_3VO_4 and resulted in effective separation of charge carriers [86]. Therefore, the BN modification will lead the improved photocatalytic activity of semiconductor/BN.

Moreover, it has been found that the ball-milled h-BN can be used as holes transfer promoter for semiconductors, such as TiO_2, ZnO and CdS [89-91]. When the semiconductor and BN contacted, the holes from semiconductor could transfer to the surface due to the negatively charged of BN. For example, h-BN/TiO_2 composite photocatalyst was prepared by ball-milling process. The transfer rate of holes from the bulk of TiO_2 to its surface can be improved by the negatively charged h-BN. The efficient holes transfer from TiO_2 to the BN resulted in the enhancement of photocatalytic activity of TiO_2.

Furthermore, porous BN has high surface area and good thermal stability. It could be used as a support material for semiconductors to enhance the photocatalytic activity [77, 92]. For porous BN/TiO_2 composite, the high BET surface area contributed to their high adsorption ability for pollutant [124]. It is important to enhance adsorption ability of a photocatalyst because the photo-induced reaction species are located on its surfaces mostly. In addition, the large surface area of porous

550 BN provides a good spatial condition for the charge transportation, thus ensuring a

551 continuous charge transfer.

552 **5. Conclusions and perspective**

553 In conclusion, this work summarized recent progress on the synthesis of BN and

554 semiconductor/BN composites. The BN can be introduced into various semiconductor

555 photocatalysts to form semiconductor/BN composites. Many methods including

556 *in-situ* growth method, ball milling method, hydrothermal and solvothermal method,

557 and thermal condensation method have been explored for the syntheses of the

558 semiconductor/BN composites. These semiconductor/BN composites have various

559 applications in photocatalytic fields, such as pollutant degradation and photocatalytic

560 hydrogen evolution. Coupling BN with semiconductors can improve the

561 photocatalytic activity of semiconductors dramatically. In addition, the role of BN in

562 semiconductor/BN composites is discussed in depth.

563 Despite the bright future of BN-based materials, there are some issues that should

564 be taken into consideration.

565 (1) Preparation of BN and BN-based nanomaterials. The preparation methods of

566 functionalized BN and BN-based nanomaterials are still rather difficult, particularly

567 compared to graphene analogues. This situation is primarily explained by high

568 chemical inertness of BN-based materials that prevent them from direct modifications.

569 A lot of synthetic methods were applied for the preparation of modified BN and

570 BN-based nanomaterials, however, the yield and efficiency of these methods are not

571 satisfied yet.

(2) Roles of BN. The roles of BN were reviewed, while it is far from completion. It is reported that the strong interaction between BN and semiconductor improves the charge separation and transfer properties in the BN-based photocatalysts. BN can promote the immigration of holes from the bulk of photocatalyst to its surface and consequently improve the photocatalytic activity. Bonds like B-O-Ti have been formed in the BN/TiO$_2$. The semiconductors properties of BN are usually overlooked. Besides, the structure of BN plays a crucial role in BN/semiconductor hybrids. 0D BN quantum dots, 1D BN nanorods and 3D BN framework have special electronic and optical properties, which are different from 2D BN nanosheet. The unique properties of BN QDs might be beneficial to separation of photoinduced charges and absorption of solar light.

(3) Theoretical calculation of BN-based materials. Many experiments demonstrated the key roles of BN in the enhancement of photocatalytic activity. However, the inherent mechanism in the enhancement of photocatalytic activity has not been figured out yet. Theoretical calculations can simulate the electronic properties and the photogenerated charge carriers at the molecular level of BN based photocatlysts, which are beneficial to give an overall understanding of the experimental results.

Acknowledgements

598   **References**

599   [1] J. Liang, Z. Yang, L. Tang, G. Zeng, M. Yu, X. Li, H. Wu, Y. Qian, X. Li, Y.

600   Luo, Chemosphere 181 (2017) 281-288.

601   [2] H. Wu, C. Lai, G. Zeng, J. Liang, J. Chen, J. Xu, J. Dai, X. Li, J. Liu, M. Chen, L.

602   Lu, L. Hu, J. Wan, Crit. Rev. Biotechnol. 37 (2017) 754-764.

603   [3] Y. Zhang, G.M. Zeng, L. Tang, J. Chen, Y. Zhu, X.X. He, Y. He, Anal. Chem. 87

604   (2015) 989-996.

605   [4] J. Wan, G. Zeng, D. Huang, L. Hu, P. Xu, C. Huang, R. Deng, W. Xue, C. Lai, C.

606   Zhou, K. Zheng, X. Ren, X. Gong, J. Hazard. Mater. 343 (2018) 332-339.

607   [5] W. Xiong, J. Tong, Z. Yang, G. Zeng, Y. Zhou, D. Wang, P. Song, R. Xu, C.

608   Zhang, M. Cheng, J. Colloid Interf. Sci. 493 (2017) 17-23.

609   [6] C. Zhou, C. Lai, P. Xu, G. Zeng, D. Huang, C. Zhang, M. Cheng, L. Hu, J. Wan,

610   Y. Liu, W. Xiong, Y. Deng, M. Wen, ACS Sustainable Chem. Eng. 6 (2018)

611   4174-4184.

612   [7] M. Cheng, G. Zeng, D. Huang, C. Yang, C. Lai, C. Zhang, Y. Liu, Chem. Eng. J.

613   314 (2017) 98-113.

614   [8] S. Zhong, C. Zhou, X. Zhang, H. Zhou, H. Li, X. Zhu, Y. Wang, J. Hazard. Mater.

615   276 (2014) 58-65.

616   [9] P. Xu, G.M. Zeng, D.L. Huang, C.L. Feng, S. Hu, M.H. Zhao, C. Lai, Z. Wei, C.

617   Huang, G.X. Xie, Sci. Total Environ. 424 (2012) 1-10.

618 [10]C. Zhou, C. Lai, P. Xu, G. Zeng, D. Huang, Z. Li, C. Zhang, M. Cheng, L. Hu, J.

619 Wan, F. Chen, W. Xiong, R. Deng, ACS Sustainable Chem. Eng. 6 (2018)

620 6941-6949.

621 [11]X. Tan, Y. Liu, G. Zeng, X. Wang, X. Hu, Y. Gu, Z. Yang, Chemosphere 125

622 (2015) 70-85.

623 [12]J.-H. Deng, X.-R. Zhang, G.-M. Zeng, J.-L. Gong, Q.-Y. Niu, J. Liang, Chem.

624 Eng. J. 226 (2013) 189-200.

625 [13]M. Chen, P. Xu, G. Zeng, C. Yang, D. Huang, J. Zhang, Biotechnol. Adv. 33

626 (2015) 745-755.

627 [14]C. Zhang, C. Lai, G. Zeng, D. Huang, L. Tang, C. Yang, Y. Zhou, L. Qin, M.

628 Cheng, Biosens. Bioelectron. 81 (2016) 61-67.

629 [15]F. Long, J.-L. Gong, G.-M. Zeng, L. Chen, X.-Y. Wang, J.-H. Deng, Q.-Y. Niu,

630 H.-Y. Zhang, X.-R. Zhang, Chem. Eng. J. 171 (2011) 448-455.

631 [16]P. Xu, G.M. Zeng, D.L. Huang, C. Lai, M.H. Zhao, Z. Wei, N.J. Li, C. Huang,

632 G.X. Xie, Chem. Eng. J. 203 (2012) 423-431.

633 [17]X. Ren, G. Zeng, L. Tang, J. Wang, J. Wan, Y. Liu, J. Yu, H. Yi, S. Ye, R. Deng,

634 Sci. Total Environ. 610 (2018) 1154-1163.

635 [18]D.-L. Huang, R.-Z. Wang, Y.-G. Liu, G.-M. Zeng, C. Lai, P. Xu, B.-A. Lu, J.-J.

636 Xu, C. Wang, C. Huang, Environmental Science and Pollution Research 22 (2015)

637 963-977.

638 [19]D. Huang, L. Liu, G. Zeng, P. Xu, C. Huang, L. Deng, R. Wang, J. Wan,

639 Chemosphere 174 (2017) 545-553.

640 [20]L. Hu, J. Wan, G. Zeng, A. Chen, G. Chen, Z. Huang, K. He, M. Cheng, C. Zhou,

641 W. Xiong, C. Lai, P. Xu, Environmental Science: Nano 4 (2017) 2018-2029.

642   [21]M. Cheng, G. Zeng, D. Huang, C. Lai, P. Xu, C. Zhang, Y. Liu, Chem. Eng. J.

643   284 (2016) 582-598.

644   [22]C. Zhang, C. Lai, G. Zeng, D. Huang, C. Yang, Y. Wang, Y. Zhou, M. Cheng,

645   Water Res. 95 (2016) 103-112.

646   [23]M. Cheng, G. Zeng, D. Huang, C. Lai, P. Xu, C. Zhang, Y. Liu, J. Wan, X. Gong,

647   Y. Zhu, J. Hazard. Mater. 312 (2016) 184-191.

648   [24]D. Huang, X. Gong, Y. Liu, G. Zeng, C. Lai, H. Bashir, L. Zhou, D. Wang, P. Xu,

649   M. Cheng, Planta   (2017) 1-11.

650   [25]J.-L. Gong, B. Wang, G.-M. Zeng, C.-P. Yang, C.-G. Niu, Q.-Y. Niu, W.-J. Zhou,

651   Y. Liang, J. Hazard. Mater. 164 (2009) 1517-1522.

652   [26]X. Li, J. Yu, S. Wageh, A.A. Al-Ghamdi, J. Xie, Small 12 (2016) 6640-6696.

653   [27]D. Huang, X. Wang, C. Zhang, G. Zeng, Z. Peng, J. Zhou, M. Cheng, R. Wang, Z.

654   Hu, X. Qin, Chemosphere 186 (2017) 414-421.

655   [28]J. Wang, Z. Yang, X. Gao, W. Yao, W. Wei, X. Chen, R. Zong, Y. Zhu, Appl.

656   Catal. B: Environ. 217 (2017) 169-180.

657   [29]X. Chen, Q. Chen, W. Jiang, Z. Wei, Y. Zhu, Appl. Catal. B: Environ. 211 (2017)

658   106-113.

659   [30]C. Lai, M.-M. Wang, G.-M. Zeng, Y.-G. Liu, D.-L. Huang, C. Zhang, R.-Z.

660   Wang, P. Xu, M. Cheng, C. Huang, Appl. Surf. Sci. 390 (2016) 368-376.

661   [31]W. Chen, Y.-X. Hua, Y. Wang, T. Huang, T.-Y. Liu, X.-H. Liu, J. Catal. 349

662   (2017) 8-18.

663   [32]C.Y. Zhou, C. Lai, D.L. Huang, G.M. Zeng, C. Zhang, M. Cheng, L. Hu, J. Wan,

664   W.P. Xiong, M. Wen, X.F. Wen, L. Qin, Appl. Catal. B: Environ. 220 (2018)

665   202-210.

666   [33]G. Mamba, A.K. Mishra, Appl. Catal. B: Environ. 198 (2016) 347-377.

667   [34]L. Jiang, X. Yuan, Y. Pan, J. Liang, G. Zeng, Z. Wu, H. Wang, Appl. Catal. B:

668   Environ. 217 (2017) 388-406.

669   [35]M. Zhang, W. Jiang, D. Liu, J. Wang, Y. Liu, Y. Zhu, Y. Zhu, Appl. Catal. B:

670   Environ.183 (2016) 263-268.

671   [36]Q. Zheng, D.P. Durkin, J.E. Elenewski, Y. Sun, N.A. Banek, L. Hua, H. Chen,

672   M.J. Wagner, W. Zhang, D. Shuai, Environ Sci. Technol. 50 (2016) 12938-12948.

673   [37]X. An, J.C. Yu, Rsc Adv. 1 (2011) 1426.

674   [38]Q. Xiang, J. Yu, M. Jaroniec, Chem. Soc. Rev. 41 (2012) 782-796.

675   [39]M. Yankowitz, K. Watanabe, T. Taniguchi, P. San-Jose, B.J. LeRoy, Nat.

676   Commun. 7 (2016) 13168.

677   [40]C. Huang, C. Li, G. Shi, Energy & Environmental Science 5 (2012) 8848.

678   [41]X.-F. Jiang, Q. Weng, X.-B. Wang, X. Li, J. Zhang, D. Golberg, Y. Bando,

679   Journal of Materials Science & Technology 31 (2015) 589-598.

680   [42]J. Wang, Y. Wu, Y. Xue, D. Liu, X. Wang, X. Hu, Y. Bando, W. Lei, J. Mater.

681   Chem. A 6 (2018) 1363-1369.

682   [43]Z. Zhang, E.S. Penev, B.I. Yakobson, Chem Soc Rev 46 (2017) 6746-6763.

683   [44]W. Peiwen, X. Shize, Z. Wenshuai, L. Hongping, C. Yanhong, Z. Huiyuan, L.

684   Huaming, D. Sheng, Small 13 (2017) 1701857.

685   [45]G. Xie, K. Zhang, B. Guo, Q. Liu, L. Fang, J.R. Gong, Adv Mater 25 (2013)

686   3820-3839.

687   [46]J. Wang, J. Hao, D. Liu, S. Qin, C. Chen, C. Yang, Y. Liu, T. Yang, Y. Fan, Y.

688   Chen, Nanoscale 9 (2017) 9787-9791.

689   [47]D. Liu, W. Lei, S. Qin, Y. Chen, Scientific Reports 4 (2014) 4453.

690   [48]L. Weiwei, L. Dan, C. Ying, Adv. Mater. Interfaces 2 (2015) 1400529.

691 [49] S.R. Naqvi, G.S. Rao, W. Luo, R. Ahuja, T. Hussain, ChemPhysChem 18 (2017)

692 513-518.

693 [50] J. Zhu, H. Wang, J. Liu, L. Ouyang, M. Zhu, Nanotechnology 28 (2017) 115604.

694 [51] J. Zhu, H. Wang, W. Cai, J. Liu, L. Ouyang, M. Zhu, International Journal of

695 Hydrogen Energy 42 (2017) 15790-15798.

696 [52] K. Zhang, Y. Feng, F. Wang, Z. Yang, J. Wang, J. Mater. Chem. C 5 (2017)

697 11992-12022.

698 [53] L. Wang, P. Hu, Y. Long, Z. Liu, X. He, J. Mater. Chem. A 5 (2017)

699 22855-22876.

700 [54] D. Liu, M.W. Zhang, W.J. Xie, L. Sun, Y. Chen, W.W. Lei, Catalysis Science &

701 Technology 6 (2016) 8309-8313.

702 [55] C. Lee, S. Bhandari, B. Tiwari, N. Yapici, D. Zhang, Y. Yap, Molecules 21 (2016)

703 922.

704 [56] Q. Weng, X. Wang, X. Wang, Y. Bando, D. Golberg, Chem. Soc. Rev. 45 (2016)

705 3989-4012.

706 [57] Z. He, C. Kim, L. Lin, T.H. Jeon, S. Lin, X. Wang, W. Choi, Nano Energy 42

707 (2017) 58-68.

708 [58] W. Lei, V.N. Mochalin, D. Liu, S. Qin, Y. Gogotsi, Y. Chen, Nature

709 Communications 6 (2015) 8849.

710 [59] Y. Wu, Y. Xue, S. Qin, D. Liu, X. Wang, X. Hu, J. Li, X. Wang, Y. Bando, D.

711 Golberg, Y. Chen, Y. Gogotsi, W. Lei, ACS Appl. Mater. Interfaces 9 (2017)

712 43163-43170.

713 [60] W. Lei, D. Portehault, D. Liu, S. Qin, Y. Chen, Nature Communications 4 (2013)

714 1777.

715 [61] W. Yingcheng, W. Peiwen, C. Yanhong, H. Jing, L. Hongping, L. Linjie, J. Wei,

716 Z. Beibei, L. Huaming, Z. Wenshuai, Nanotechnology 29 (2018) 025604.

717 [62] D. Lee, B. Lee, K.H. Park, H.J. Ryu, S. Jeon, S.H. Hong, Nano Letters 15 (2015)

718 1238-1244.

719 [63] W.-Q. Han, R. Brutchey, T.D. Tilley, A. Zettl, Nano Letters 4 (2004) 173-176.

720 [64] Z. Tong, D. Yang, Z. Li, Y. Nan, F. Ding, Y. Shen, Z. Jiang, ACS Nano 11

721 (2017) 1103-1112.

722 [65] P. Dibandjo, L. Bois, F. Chassagneux, D. Cornu, J.M. Letoffe, B. Toury, F.

723 Babonneau, P. Miele, Adv. Mater. 17 (2005) 571-574.

724 [66] A. Vinu, M. Terrones, D. Golberg, S. Hishita, K. Ariga, T. Mori, Chem. Mater.

725 17 (2005) 5887-5890.

726 [67] S. Schlienger, J. Alauzun, F. Michaux, L. Vidal, J. Parmentier, C. Gervais, F.

727 Babonneau, S. Bernard, P. Miele, J.B. Parra, Chem. Mater. 24 (2012) 88-96.

728 [68] M. Maleki, A. Beitollahi, J. Javadpour, N. Yahya, Ceramics International 41

729 (2015) 3806-3813.

730 [69] J. Li, X. Xiao, X. Xu, J. Lin, Y. Huang, Y. Xue, P. Jin, J. Zou, C. Tang, Scientific

731 Reports 3 (2013) 3208.

732 [70] P. Wu, W. Zhu, Y. Chao, J. Zhang, P. Zhang, H. Zhu, C. Li, Z. Chen, H. Li, S.

733 Dai, Chem. Commun. 52 (2016) 144-147.

734 [71] Q. Li, T. Yang, Q. Yang, F. Wang, K.-C. Chou, X. Hou, Ceramics International

735 42 (2016) 8754-8762.

736 [72] A. Nag, K. Raidongia, K.P.S.S. Hembram, R. Datta, U.V. Waghmare, C.N.R.

737 Rao, ACS Nano 4 (2010) 1539-1544.

738 [73] S. Marchesini, A. Regoutz, D. Payne, C. Petit, Microporous & Mesoporous

739 Materials 243 (2017) 154-163.

[74]S. Marchesini, C.M. McGilvery, J. Bailey, C. Petit, ACS Nano 11 (2017) 10003-10011.

[75]C. Tang, J. Li, Y. Bando, C. Zhi, D. Golberg, Chemistry, an Asian journal 5 (2010) 1220-1224.

[76]Y. Ide, F. Liu, J. Zhang, N. Kawamoto, K. Komaguchi, Y. Bando, D. Golberg, J. Mater. Chem. A 2 (2014) 4150.

[77]D. Liu, M. Zhang, W. Xie, L. Sun, Y. Chen, W. Lei, Appl. Catal. B: Environ. 207 (2017) 72-78.

[78]M. Wang, M. Li, L. Xu, L. Wang, Z. Ju, G. Li, Y. Qian, Catal. Sci. Technol. 1 (2011) 1159.

[79]J. Choi, D.A. Reddy, T.K. Kim, Ceramics International 41 (2015) 13793-13803.

[80]W. Wu, X. Lv, J. Wang, J. Xie, J. Colloid Interf. Sci. 496 (2017) 434-445.

[81]H. Wang, X. Qiao, J. Chen, X. Wang, S. Ding, Materials Chemistry and Physics 94 (2005) 449-453.

[82]C. Zhu, J. Zheng, L. Fang, P. Hu, Y. Liu, X. Cao, M. Wu, J. Mol. Catal. A-Chem. 424 (2016) 135-144.

[83]J. Chen, J. Zhu, Z. Da, H. Xu, J. Yan, H. Ji, H. Shu, H. Li, Appl. Surf. Sci. 313 (2014) 1-9.

[84]X.-f. Wu, Z.-h. Zhao, Y. Sun, H. Li, C.-x. Zhang, Y.-j. Wang, Y. Liu, Y.-d. Wang, X.-y. Yang, X.-d. Gong, J. Nanopar. Res. 19 (2017).

[85]J. Wang, J. Shen, D. Fan, Z. Cui, X. Lü, J. Xie, M. Chen, Mater. Lett. 147 (2015) 8-11.

[86]X. Lv, J. Wang, Z. Yan, D. Jiang, J. Liu, J. Mol. Catal. A-Chem. 418 (2016) 146-153.

764 [87]L. Jiang, X. Yuan, G. Zeng, Z. Wu, J. Liang, X. Chen, L. Leng, H. Wang, H.

765 Wang, Appl. Catal. B: Environ. 221 (2018) 715-725.

766 [88]Z. He, C. Kim, L. Lin, T.H. Jeon, S. Lin, X. Wang, W. Choi, Nano Energy 42

767 (2017) 58-68.

768 [89]X. Fu, Y. Hu, Y. Yang, W. Liu, S. Chen, J. Hazard. Mater. 244 (2013) 102-110.

769 [90]X. Fu, Y. Hu, T. Zhang, S. Chen, Appl. Surf. Sci. 280 (2013) 828-835.

770 [91]R. Zhang, J. Wang, P. Han, J. Alloys Compd. 637 (2015) 483-488.

771 [92]W. Xie, M. Zhang, D. Liu, W. Lei, L. Sun, X. Wang, ACS Sustainable Chem.

772 Eng. 5 (2017) 1392-1399.

773 [93]Z. Chen, X. Chen, J. Di, Y. Liu, S. Yin, J. Xia, H. Li, J. Colloid Interf. Sci. 492

774 (2017) 51-60.

775 [94]J. Di, J. Xia, M. Ji, B. Wang, S. Yin, Q. Zhang, Z. Chen, H. Li, Appl. Catal. B:

776 Environ. 183 (2016) 254-262.

777 [95]B. Wang, J. Di, J. Xia, L. Xu, H. Xu, Q. Zhang, Z. Chen, H. Li, Mater. Technol.

778 31 (2016) 463-470.

779 [96]D. Liu, Z. Jiang, C. Zhu, K. Qian, Z. Wu, J. Xie, Dalton Trans. 45 (2016)

780 2505-2516.

781 [97]S. Ding, D. Mao, S. Yang, F. Wang, L. Meng, M. Han, H. He, C. Sun, B. Xu,

782 Appl. Catal. B: Environ. 210 (2017) 386-399.

783 [98]S. Meng, X. Ye, X. Ning, M. Xie, X. Fu, S. Chen, Appl. Catal. B: Environ. 182

784 (2016) 356-368.

785 [99]X. Li, F. Qi, Y. Xue, C. Yu, H. Jia, Y. Bai, S. Wang, Z. Liu, J. Zhang, C. Tang,

786 Rsc Adv. 6 (2016) 99165-99171.

787 [100] J. Gu, J. Yan, Z. Chen, H. Ji, Y. Song, Y. Fan, H. Xu, H. Li, Dalton

788 Transactions 46 (2017) 11250-11258.

789 [101] M. Sun, Q. Fu, L. Gao, Y. Zheng, Y. Li, M. Chen, X. Bao, Nano Research 10

790 (2017) 1403-1412.

791 [102] L. Gao, Y. Wang, H. Li, Q. Li, N. Ta, L. Zhuang, Q. Fu, X. Bao, Chem. Sci.

792 8 (2017) 5728-5734.

793 [103] N. Sagara, S. Kamimura, T. Tsubota, T. Ohno, Appl. Catal. B: Environ. 192

794 (2016) 193-198.

795 [104] C. Huang, C. Chen, M. Zhang, L. Lin, X. Ye, S. Lin, M. Antonietti, X. Wang,

796 Nature Commun. 6 (2015) 7698.

797 [105] S. Thaweesak, S. Wang, M. Lyu, M. Xiao, P. Peeraktukajohn, L. Wang,

798 Dalton Transactions 46 (2017) 10714-10720.

799 [106] M. Nasr, R. Viter, C. Eid, R. Habchi, P. Miele, M. Bechelany, New Journal

800 of Chemistry 41 (2017) 81-89.

801 [107] H. Xu, Z. Wu, M. Ding, X. Gao, Materials & Design 114 (2017) 129-138.

802 [108] B. Singh, G. kaur, P. Singh, K. Singh, J. Sharma, M. Kumar, R. Bala, R.

803 Meena, S.K. Sharma, A. Kumar, New Journal of Chemistry 41 (2017) 11640-11646.

804 [109] H. Si, G. Lian, J. Wang, L. Li, Q. Wang, D. Cui, C.P. Wong, ACS Appl.

805 Mater. Interfaces 8 (2016) 1578-1582.

806 [110] D. Liu, W. Cui, J. Lin, Y. Xue, Y. Huang, J. Li, J. Zhang, Z. Liu, C. Tang,

807 Catal. Commun. 57 (2014) 9-13.

808 [111] X.-F. Wu, H. Li, Y. Sun, Y.-J. Wang, C.-X. Zhang, J.-Z. Su, J.-R. Zhang,

809 F.-F. Yang, Y. Zhang, J.-C. Pan, Appl. Phy. A 123 (2017) 709.

810 [112] J. Yan, J. Gu, X. Wang, Y. Fan, Y. Zhao, J. Lian, Y. Xu, Y. Song, H. Xu, H.

811 Li, Rsc Adv. 7 (2017) 25160-25170.

812 [113] F. Ma, G. Zhao, C. Li, T. Wang, Y. Wu, J. Lv, Y. Zhong, X. Hao,

813 CrystEngComm 18 (2016) 631-637.

814 [114] C. Zhu, J. Zheng, L. Fang, P. Hu, Y. Liu, X. Cao, M. Wu, Journal of

815 Molecular Catalysis A: Chemical 424 (2016) 135-144.

816 [115] M. Ji, J. Xia, J. Di, Y. Liu, R. Chen, Z. Chen, S. Yin, H. Li, Chem. Eng. J.

817 331 (2018) 355-363.

818 [116] W. Li, Q. Wang, L. Huang, Y. Li, Y. Xu, Y. Song, Q. Zhang, H. Xu, H. Li,

819 Rsc Adv. 5 (2015) 88832-88840.

820 [117] S. Ding, D. Mao, S. Yang, F. Wang, L. Meng, M. Han, H. He, C. Sun, B. Xu,

821 Appl. Catal. B: Environ. 210 (2017) 386-399.

822 [118] H. Xu, Z. Wu, M. Ding, X. Gao, Materials & Design 114 (2017) 129-138.

823 [119] W. Xie, M. Zhang, D. Liu, W. Lei, L. Sun, X. Wang, Journal of

824 Photochemistry and Photobiology A: Chemistry 333 (2017) 165-173.

825 [120] X. Wang, K. Maeda, A. Thomas, K. Takanabe, G. Xin, J.M. Carlsson, K.

826 Domen, M. Antonietti, Nat. mater. 8 (2009) 76-80.

827 [121] Y. Wang, X. Wang, M. Antonietti, Angew. Chem. Int. Ed. 51 (2012) 68-89.

828 [122] L. Jiang, X. Yuan, G. Zeng, J. Liang, X. Chen, H. Yu, H. Wang, Z. Wu, J.

829 Zhang, T. Xiong, Appl. Catal. B: Environ. 227 (2018) 376-385.

830 [123] L. Jiang, X. Yuan, G. Zeng, Z. Wu, J. Liang, X. Chen, L. Leng, H. Wang, H.

831 Wang, Appl. Catal. B: Environ. 221 (2018) 715-725.

832 [124] V. Štengl, J. Henych, M. Slušná, J. Nanomater. 2016 (2016) 1-12.

833

834   Figure captions

835   Fig.1. (a) Thin curled sheets peeling off the top surface of an h-BN particle in

836   response to shear forces created by the milling balls. (b)Low-magnification TEM

837   image of OH-BNNPs and corresponding selected-area diffraction (SAED) patterns.

838   Reproduced with permission from Ref. [62]. Copyright 2015, ACS.

839   Fig.2. Overall synthetic path employed to generate zeolite-derived BN-based

840   materials with micro- and mesoporosity. Note that the last structure is in fact

841   disorganized. Reproduced with permission from Ref. [68]. Copyright 2011, ACS.

842   Fig. 3. Template-free synthesis methods for porous boron nitride using (a) a single

843   N-containing precursor route; (b) a two N-containing precursors route.

844   Fig.4. TEM images of (a) porous BNNSs and (b) porous BN/TiO$_2$ hybrid nanosheets

845   (TiO$_2$: 38 wt%). (c) and (d) HRTEM images for a hole decorated by TiO$_2$

846   nanoparticles from the rectangular area in (b), and a single TiO$_2$ particle as indicated

847   by the white arrow in (c). Reproduced with permission from Ref.[78]. Copyright 2017,

848   elsevier.

849   Fig.5. Schematic illustration of the synthetic process for (a) graphene-analogue h-BN

850   and (b) h-BN/Bi$_4$O$_5$Br$_2$ composites. Reproduced with permission from Ref. [97].

851   Copyright 2017, Elsevier.

852   Fig.6. (a, b) TEM images of TiO$_2$@BN(80) hollow nanospheres hybrid. (c) HRTEM

853   image of TiO$_2$ NCs. Inset shows the magnified interplanar spaces of TiO$_2$ labeled. (d)

854   Photocatalytic degradation curves of MO with BN, TiO$_2$ NCs, TiO$_2$@BN(50), and

855   TiO$_2$@BN(80). (e) FTIR spectra of MO, TiO$_2$@BN hybrids before and after reaction.

856   Reproduced with permission from Ref.[109]. Copyright 2017, ACS.

857 Fig. 7. (a) Photodegradation of RhB by BiOBr and graphene-like BN/BiOBr

858 composites under visible light irradiation; (b) time-dependent UV–vis absorption

859 spectra in the presence of 1 wt% graphene-like BN/BiOBr. (c) Photodegradation of

860 RhB by BiOI and graphene-like BN/BiOI composites under visible light irradiation.

861 (d) Variations in the characteristic absorption of RhB under visible light irradiation

862 using 0.5 wt% BN/BiOI. (a-b) Reproduced with permission from Ref.[96]. Copyright

863 2016, Elsevier. (c-d) Reproduced with permission from Ref.[94]. Copyright 2017,

864 Elsevier.

865 Fig. 8. Crystal structures, calculated band structures and density of states of (a, b)

866 $Bi_4O_5Br_2$ and (c, d) h-BN. (e) Schematic of the separation and transportation of

867 photo-induced charges in the h-BN/$Bi_4O_5Br_2$ composite combined with the possible

868 photocatalytic degradation mechanism. Reproduced with permission from Ref.[117].

869 Copyright 2017, Elsevier.

870 Fig. 9. Possible photocatalytic mechanism of RhB (a) and TC (b) degradation by 2D

871 BN/g-C_3N_4. (a) Reproduced with permission from Ref. [100]. Copyright 2017,

872 Elsevier. (b) Reproduced with permission from Ref. [123]. Copyright 2018, Elsevier.

873 Fig. 10. (a-b) TEM images and EELS mapping data of CBN-6, (c) Time profiles of

874 photocatalytic H_2 production in the presence of BN, CN or CBN-x samples.

875 (d)Determined band energy levels of CBN-x electrodes , in comparison with pure

876 h-BN and CN electrodes. The standard reduction potentials for H^+/H_2, O_2/H_2O_2 and

877 O_2/H_2O couples are shown as a reference. Reproduced with permission from Ref. [57].

878 Copyright 2017, Elsevier.

879